Published in Microelectronic Engineering ©, Volume 217, 111129 (2019) **DOI:** 10.1016/j.mee.2019.111129

Portable optical blood scattering sensor

Konstantinos Karakostas[a, *], Stratos Gkagkanis[b], Korina Katsaliaki[c], Peter Köllensperger[d], Alkiviadis Hatzopoulos[a] and Michail E. Kiziroglou[b, e]

[a] *Department of Electrical and Computer Engineering, Aristotle University of Thessaloniki, Thessaloniki, 54124, Greece*
[b] *Department Automation Engineering, Alexander Technological Educational Institute of Thessaloniki, Sindos, 57400, Greece*
[c] *School of Economics, Business Administration and Legal Studies, International Hellenic University, Thermi, 57001, Greece*
[d] *NanoLab, Norwegian University of Science and Technology, Trondheim, 7491, Norway*
[e] *Department of Electrical and Electronic Engineering, Imperial College London, London, SW7 2AZ, United Kingdom*

*Corresponding author.
E-mail address: karakosk@ece.auth.gr

Received 13 June 2019; Received in revised form 11 August 2019; Accepted 26 August 2019
Available online 26 August 2019

A B S T R A C T

Modern non-invasive medical sensors can continuously provide vital information such as blood oxygenation, hemoglobin and glucose, based on substance-specific spectral or electrochemical properties. Cells and other geometrical formations are difficult to observe non-invasively due to the absence of a distinctive substantial signature. Optical scattering angle measurements could provide geometrical information but multiple scattering results in diffusion profiles, limiting their direct applicability. Mie scattering correlation to blood cell size has been demonstrated in the lab and various biomedical optical techniques are under intense investigation towards decoupling direct from indirect scattering, requiring specialized equipment. In this paper, a portable sensor is introduced for in-vitro and potentially in-vivo study of light scattering from blood. A microcontroller-based prototype has been designed and fabricated, with a 650 nm laser source, a 128 × 1 photodiode array and a custom dual-core real-time data acquisition algorithm. The prototype has been evaluated using latex sphere solutions calibrated to emulated red blood cells, white blood cells and platelets. Distinct scattering signatures are demonstrated for the three blood cell sizes. Reproducibility and repeatability tests analyzing data from multiple independent experiments demonstrate the reliability of the demonstration. This device platform provides a flexible and simple means for evaluating optical processing methods towards non-invasive continuous counting of blood cells.

A R T I C L E I N F O

Keywords: Mie scattering, blood cells, microcontroller, non-invasive, sensor, health monitoring

1. Introduction

Non-invasive technologies for monitoring human health are expected to drastically improve life quality and open up new possibilities in medicine. Examples of benefits include simplification of medical practices, reduction of invasive probing and the associated health risks, patient comfort improvement as well as cost-effective and fast examination, monitoring and treatment services. In addition, frequent or continuous monitoring of health parameters over time can revolutionize the treatment of chronic medical conditions, both through personalised care and data analysis for treatment-response correlation. An example of the impact that continuous monitoring can be found in the glucose monitoring and closed loop insulin delivery technology, which has improved the life quality of millions of people with diabetes in the last decade [1-3]. Continuous counting of blood cell concentrations could be equally beneficial for medical cases where cell counting is critical, such as in conditions related to anemia, leukopenia, leucocytosis, thrombocytosis or thrombocytopenia.

Existing non-invasive systems are able to measure medical indicators such as oxygenation [4, 5], bilirubin [6] and hemoglobin [7] by spectrophotometric methods, and

glucose by electrochemical analysis of epidermal fluids [2]. These methods are difficult to use directly for cell concentration, but they provide significant background knowledge and a range of valuable techniques for sensor design and development, signal detection and processing and data interpretation.

Light scattering has been shown in the lab, using large scale equipment, to provide a different signature for different cell sizes, due to a Mie scattering mechanism [8]. Mie scattering refers to the elastic scattering of light from particles whose diameter is similar to or larger than the wavelength of the incident light. A detailed description and full mathematical analysis of Mie scattering were given by Bohren and Huffman [9]. The difference in scattering profile due to different cell size, is illustrated by simulation using the MiePlot simulation software in Fig. 1 [10, 11]. The Mie profile repeating wave period as a function of particle size is shown in the inset, demonstrating the size / angle profile correspondence. Based on this mechanism, we have previously proposed a portable device design for monitoring blood cell concentration [10].

While this is a very promising correlation for non-invasive in-vivo sensing, the small photon mean free path in tissue, in the 0.1 mm scale [12], obstructs its use. Light undergoes multiple scattering even through short distances on the tissue surface, resulting in very weak directionality and diffusive profiles. Significant research effort has been invested in studying and separating single from multiple scattering effects towards advanced optical sensing [13]. Polarization gating has been shown to distinguish between surface and deep backscattering, utilizing the level of depolarization of polarized photons. Circular polarization has been shown to be advantageous in this direction due to its lower relaxation through multiple scattering events [14]. Interferometry has also been used to obtain the scattering angle profile at different penetration depths, by a backscattering measurement setup [15]. The combination of scattering spectroscopy with confocal microscopy, to allow the detection of scattering from only a specific target volume through a pinhole has also been proposed [16, 17]. On the other hand, diffusive scattering and optical spectroscopy can also provide significant information on the size of cellular structures [13, 18].

While research on these methods has been growing rapidly in recent years, experiments often involve large scale and high cost specialized optical equipment. Portable optical analysis sensors would offer flexibility and practicality in method testing. This is especially true for in-vivo measurements, where exploitable mechanisms such as blood flow are difficult to emulate in the lab. In contrast to the market of end-user biomedical devices, where a variety of portable products is available, portable laboratory equipment is not as diverse, typically limited to established optical methods. Previously reported portable devices for optical-scattering biomedical sensing include a low-coherence interferometry device for nuclear size detection [19], and a portable device design for sensing scattering on blood cells [10].

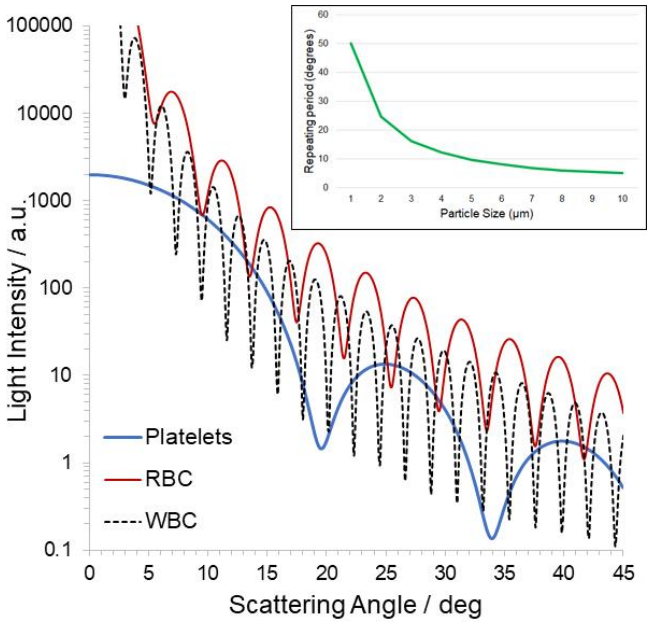

Fig. 1. Indicative simulated Mie scattering from blood cells using the MiePlot software [10, 11]. The inset shows the relation between cell size and angle profile.

In this framework, a flexible and cost-effective optical sensor platform that would permit implementation and testing of various promising methods and their combination both in laboratory and in-vivo, would be highly desirable. Here, such a portable device platform is proposed, with the potential of using multiple light sources and detector geometries, to allow diffusion and scattering characterization. A specific implementation for measuring the angle distribution of scattered light through blood samples is presented. Its capability of distinguishing among blood cell calibration solutions, from their light scattering profile is demonstrated. The repeatability and the reproducibility of the results is evaluated by multiple test runs. Finally, the potential of such methods towards non-invasive blood cell concentration monitoring is briefly discussed.

2. Sensing concept

The proposed sensing concept is illustrated in Fig. 2. A directional light source is used through a blood-carrying specimen. The light is scattered by blood cells as well as by other structures towards different angles. The size of blood cells relative to the wavelengths of visible light correspond to Mie scattering. The intensity of Mie scattering is a wave-like function of angle, with an oscillating period and amplitude depending on the particle size and refractive index, as shown in the simulation data of Fig. 1. Single event scattering is extremely rare, and multiple scattering is expected to dominate, resulting in a diffusion angle profile, especially in

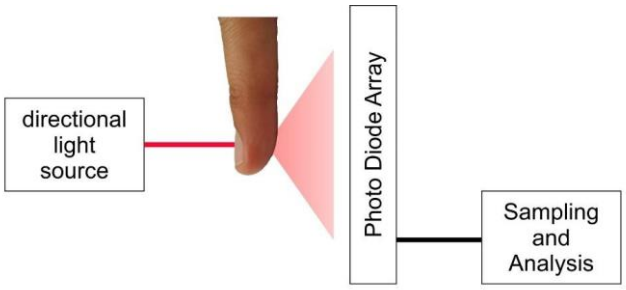

Fig. 2. Illustration of the scattering-angle analysis sensing concept.

the case of in-vivo measurements. Nevertheless, the scattered light angle profile contains significant geometrical information and can be enhanced by optical filtering. The profile can be measured over time using a photo detector array. Optical polarization and directionality filters can be used such as to amplify the Mie scattering signal or to enhance light scattered from a specific region. The acquired measurements can be analysed, providing information on the cell size distribution.

For in-vivo measurements, similarly to pulse oximetry, the blood volume changes in the microvascular bed of tissue and hence the pulse profile can be detected by the average light intensity across the array over time. Then, by subtraction between the image frames at maximum and minimum capillary volume, a differential measurement of the blood scattering profile can be obtained. This technique could be combined with other non-invasive sensing techniques such as occlusion [20, 21].

3. The prototype system

3.1 Hardware setup

A block diagram of the prototype system is illustrated in Fig. 3. As lighting source, a SYD1230 class 3a red laser pointer has been chosen with an emission wavelength of 650 nm, a power of 5 mW and a spot diameter of around 1 mm. The photodiode array (PDA) sensor, an AMS AG TSL 1401CL chip, was placed at a distance of 50 mm away from the laser pointer. This PDA sensor contains an array of 128 x 1 photodiodes with an active area length of 8.064 mm and analog output. The PDA captures the intensity of light at different positions across its length, thereby acquiring a profile of light intensity over a range of scattering angles. For each frame, all photodiodes of the PDA accumulate charge into capacitors during a light exposure interval. Subsequently the voltage of each one is sequentially provided to the PDA chip output by switching, where it is sampled by the system's analog-to-digital converter. The full specifications of this device can be found in [22].

The laser pointer was manually calibrated to aim at the edge of the PDA, by running no-specimen measurements, and selecting the position such that only the first few pixels are saturated by the laser. This geometry technique was

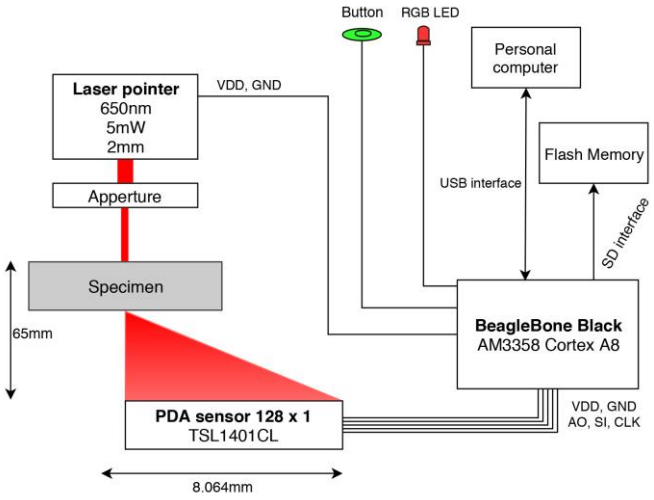

Fig. 3. Block diagram of the proposed system.

chosen in order to increase the range of the measured scattering angle.

For PDA and laser driving, data acquisition and analysis, the BeagleBone Black (BBB) development platform was used, with an AM3358 System on Chip (SoC), housing an ARM Cortex A8 and two Programmable Realtime Units (PRUs). The full specifications of this device can be found in [23]. The BBB delivers 5 V powering voltage to the laser diode and 3.3 V to the PDA sensor. It includes an integrated 12-bit analog to digital converter (ADC) in an input voltage range between 0-1.8 V.

The PDA's output voltage range is 0-3.3 V, and therefore it was adapted to the ADC input range by a voltage divider. To avoid any possible impedance problems, buffer operational amplifiers, with a slew rate of 350V/μs, (LT1810 - Linear Technologies [24]) were placed before and after the voltage divider. Decoupling and filtering capacitors were also used.

All these components are arranged in a single PCB, designed to fit the BBB cape interface. The implemented circuit is shown in Fig. 4.

While local data storage and analysis is possible in the BBB architecture, external data analysis was preferred for practical reasons during the device evaluation tests. Therefore, the optical frames are time stamped and stored in the BBB's flash memory card. The acquired measurements are transferred to a computer for subsequent data analysis via USB connection. The USB interface is also used for powering the BBB with 5 V. Once the BBB is programmed, data scanning is triggered by an external button and an RGB LED is used to indicate the status of the scanning activity.

The whole system is attached on a temporary plexiglass structure as shown in Fig. 5a. A customized housing of the device providing protection, optical shielding and easy specimen fitting was 3D printed using acrylonitrile butadiene styrene (ABS) and it is presented in Fig. 5b.

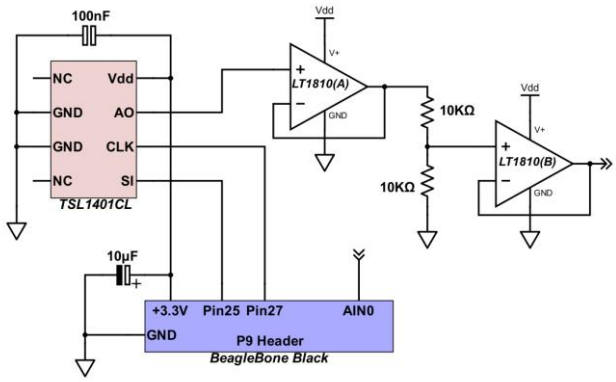

Fig. 4. Schematic diagram of the sensor's circuit.

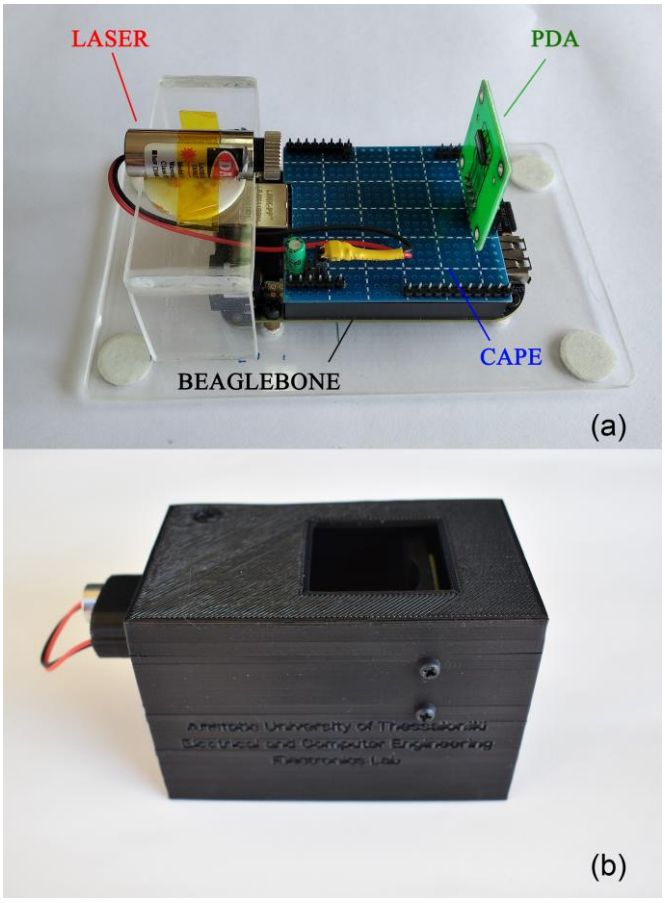

Fig. 5. (a) Photograph showing the prototype device with a specimen been in place and (b) Photograph showing the 3D printed housing.

3.2 Software setup

The functional requirements of the proposed system include the deterministic acquisition and accurate time stamping of frames with programmable exposure time and frame rate. For each frame, the analog-to-digital conversion of 128 values is required, at a high (clocking) speed to minimize delay between pixels. This is important to maintain a uniform exposure time as well as to suppress any motion effects to a frame.

In order to address the requirements, a custom parametric driver for the photodiode array was developed, utilizing both the 200 MHz PRUs of the BBB. The PRU0 remains in deterministic operation throughout, driving the digital signals of the PDA. The PRU1 controls the ADC and stores the data to the RAM, for collection by the ARM processor after the completion of the sampling run. The PRU0 triggers each ADC sampling by sending an interrupt to PRU1. The high clocking speed of the PRUs and the ADC ensures negligible delay between samples, in the range of a few tens of nanoseconds. This is negligible in comparison to the A/D conversion time which is 625 ns, as well as to the PDA integration time, which for this application is in the 36-60 µs range. The maximum framerate is therefore limited by the required exposure time for a given set of light source, specimen and environmental lighting conditions.

The driver software was developed as an integrated routine, with a four-argument input vector. The vector consists of the number of frames to be captured, integration time in microseconds, frames per second (fps) and the frequency of the PDA's CLK signal in kHz.

The algorithm checks whether the values given are within the acceptable range and continues by calculating the number of clock cycles for the PRU delay routines. The next step for the ARM processor is to write the calculated data to the predefined addresses in RAM and load each PRU with its corresponding code file. After the PRUs complete their initializations, a three-way handshake takes place in order to synchronize the CPUs. When the driving procedure is complete, the ARM collects the captured frames from the shared RAM and saves them in text file format into the flash memory. The implement algorithm is shown in Fig. 6.

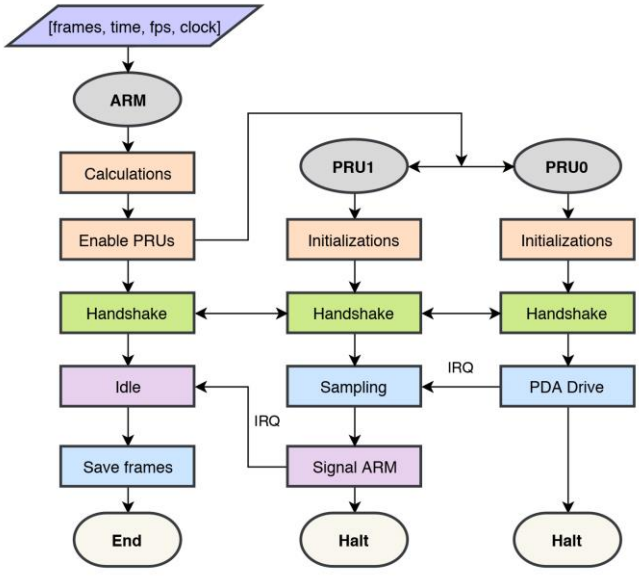

Fig. 6. Block diagram of the system software.

4. Evaluation

4.1 System configuration and data acquisition

The system's ability to distinguish Mie scattering from cells of different sizes was tested using calibration buffers containing particles with size almost similar to that of normal blood cells. At this point there is no need for using particles with diameter exactly the same as that of the blood cells. Specifically, the samples used for calibration are monodisperse polystyrene spheres in aqueous suspensions with a nominal diameter of 2 μm (BCR-165), 4.8 μm (BCR-166) and 9.6 μm (BCR-167). The particle concentration is approximately 30 x 10^9 particles/L [25]. Three different samples were prepared, each one containing a different particle size. The samples were placed in rectangular glass cuvettes with a light travel distance of 10 mm. All the cuvettes were cleaned carefully with distilled water and blow-dried. For each sample, 0.1 ml of polystyrene spheres were injected into the bottom of the cuvette using a syringe. Also 0.8ml of distilled water were added into the cuvette, thus creating a 1/8 ratio solution (the particle concentration is approximately 3750 particles/μL). Other dilution rates were also used to evaluate the ability of the system to characterize high and low particle concentrations. These solutions were then mixed well into the cuvette. All the samples were prepared and measured at room temperature.

The cuvettes were placed between the PDA sensor and the laser diode at a distance of 25 mm and 20 mm respectively. This distance allows monitoring scattering angles between 0° and 15°, enough to extract conclusions about the measured particle size, as it will be shown in the next subsection of this paper. The laser beam aims the cuvette at its center at an angle of 90° with respect to the glass surface. To minimize ambient light noise, temporary special canopies were constructed around the cuvette and the PDA sensor. The canopies consist of black cardboard, internally coated with velvet paper to minimize light reflection from the cuvette and the cardboard itself. The canopies were placed as close as possible to the PDA and the cuvette with a maximum distance of 20 mm. The PDA's PCB (showed in green at Figure 5a) was covered (except the sensor) with velvet paper too.

The measuring setup using the 3D-printed housing is shown in Fig. 7. For placing the cuvette at the right height, a 3D-printed calibration platform was attached to the cape. This setup was used for all measurements.

For each measurement, an acquisition duration of five seconds was used, in which the PDA sensor collected 40 frames per second. Hence, each measurement comprises 200 frames of 128 12-bit samples per frame. The PDA optical exposure (charge integration) time was 38 μs for all experiments presented in this section. This value was experimentally determined to provide a good signal-to-noise ratio for the specific setup, parameters and conditions.

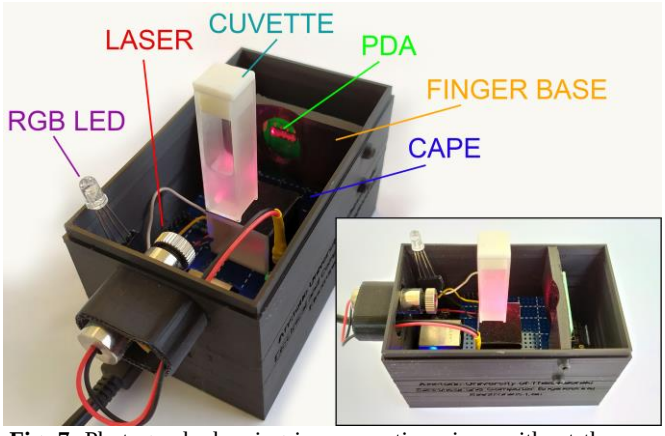

Fig. 7. Photograph showing in perspective view, without the cap, the measuring setup using the 3D printed housing. A top-front view is shown in the inset.

The laser power was kept at 5 mW for all the experiments as well.

The frequency of the PDA clock signal was chosen at 100 kHz for all experiments.

In total, 15 indicative experiments are presented, 5 for each sample. After each measurement the buffer samples were allowed to sedimentate and they were subsequently shaken well, before the next measurement. Using this method, several experiments (over 200) were performed in order to evaluate the repeatability and the reproducibility of the device measurements.

4.2 Experimental results

For the processing and the plotting of the signals, the data text file was loaded into Matlab. From the 200 frames that were collected by the PDA sensor, 50 of them were chosen randomly for processing. All the frames were converted into analog signals. Voltage is the unit of measurement for these signals (PDA's output), but they correspond to arbitrary units for light intensity. Taking the average for each bit of the fifty frames including a signal smoothing technique (median filtering), results in the blue lines as shown in Fig. 8.

As mentioned in section 1, at this particle size, Mie scattering is expected to dominate. In order to evaluate the obtained experimental results against the Mie theory, simulations were run using the diffraction software MiePlot. The refractive index values used were 1.59 for polystyrene spheres [26] and 1.33 for the medium (distilled water) [27]. A light wavelength of 650 nm was assumed and the light source type was set point-type, with parallel polarization, and a monodisperse particle solution. The maximum angle was chosen at 15° with an angular resolution of 0.1, in line with the experimental conditions. The Mie simulations and the measured data are plotted together in Fig. 8. No parameter fitting was used, in order to provide a direct comparison using only nominal values for refractive index and particle size. The deviation from a wave-like scattering

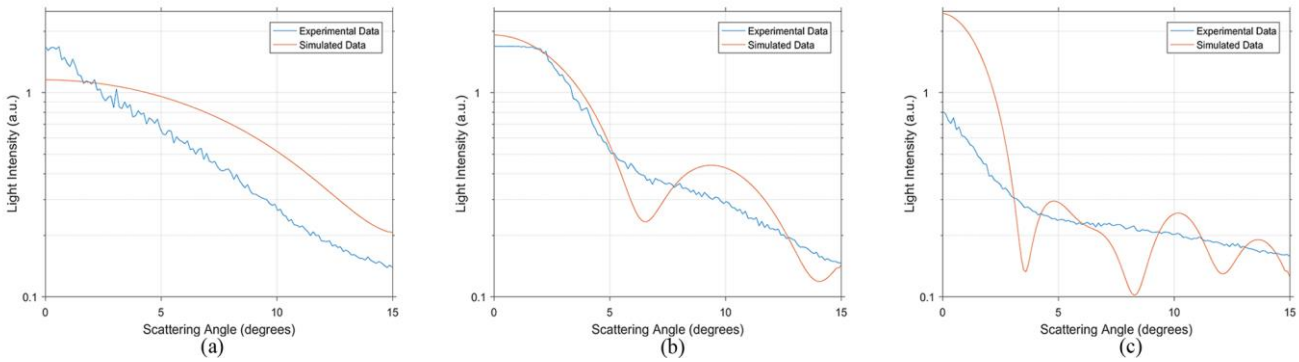

Fig. 8. Calculated primary Mie scattering profiles for polystyrene spheres with a diameter of (a) 2 μm, (b) 4.8 μm and (c) 9.6 μm, plotted against the corresponding experimental measurements.

profile is attributed to the high concentration of the solutions under study which results in multiple scattering, thereby weakening the primary Mie signature. However, some similarity in overall trend between the measurements and the Mie theory is observed, in the 2 μm and 4.8 μm solutions.

For the 9.6 μm spheres, the larger size results in higher density for the given 1/8 concentration. As a result, the intensity and the resolution of the scattered light wave drops significantly. In Fig. 9, scattering measurements are presented for six different solutions using 9.6 μm diameter spheres. As the dilution rate increases, the concentration becomes lower, which leads to a sharper fall and a more pronounced curvature of the scattering angle profile between 0° and 5°. This corresponds well to the simulated Mie profile at this angle range.

In Fig. 10, the experimental measurements of Fig. 8 are re-plotted in the same diagram for comparison. The measured angle profile from distilled water is also included for reference. A distinct signature for each particle size is observed. This result demonstrates the ability of the implemented system to detect and distinguish different particle sizes at the μm diameter range, corresponding to the average size of different blood cells. The reproducibility and repeatability of this results are evaluated by multiple experiments in the following subsection.

4.3 Repeatability and reproducibility

In order to evaluate the distinguishing ability of the implemented system, the reproducibility and the repeatability had to be examined. Reproducibility refers to the variation in measurements made on a subject under changing conditions. Conversely, repeatability of measurements refers to the variation in repeated measurements made on the same subject under the same conditions, over a short time period.

To assess the reproducibility of the results, the experiments described in the previous sections were repeated five times during different conditions including time of day, date and temperature. The results for each particle size are shown in Fig. 11. Significant reproducibility is observed.

To investigate the distribution of the collected data, histograms for each bit were constructed and merged into a single 3D plot. In Fig. 12 the 3D histogram plots are presented for each particle size. The X-axis represents the scattering angle, while the Y and Z axes represent light intensity grouped

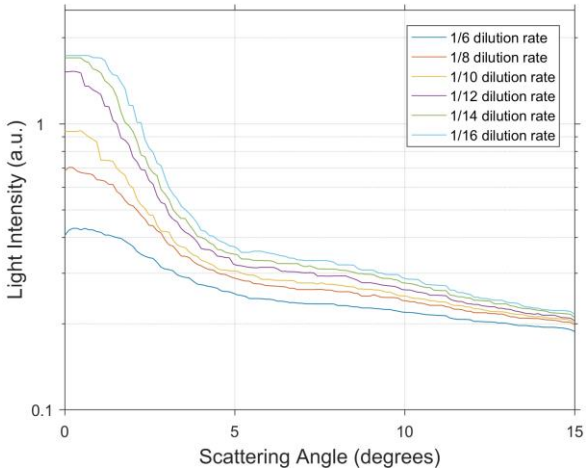

Fig. 9. Measured scattering angle profile results for 6 different dilution rates on solutions with 9.6 μm particle diameter.

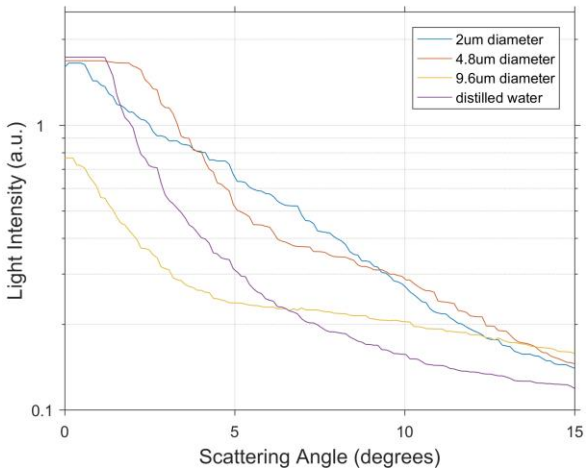

Fig. 10. Comparison between the three different diameter polystyrene particles and distilled water.

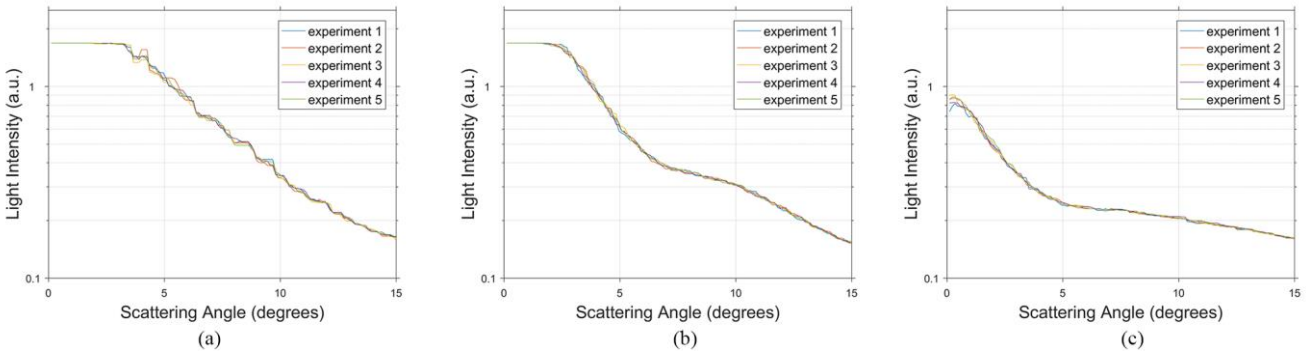

Fig. 11. Reproducibility of the measurements during five different experiments for each particle size (a) 2 μm, (b) 4.8 μm and (c) 9.6 μm

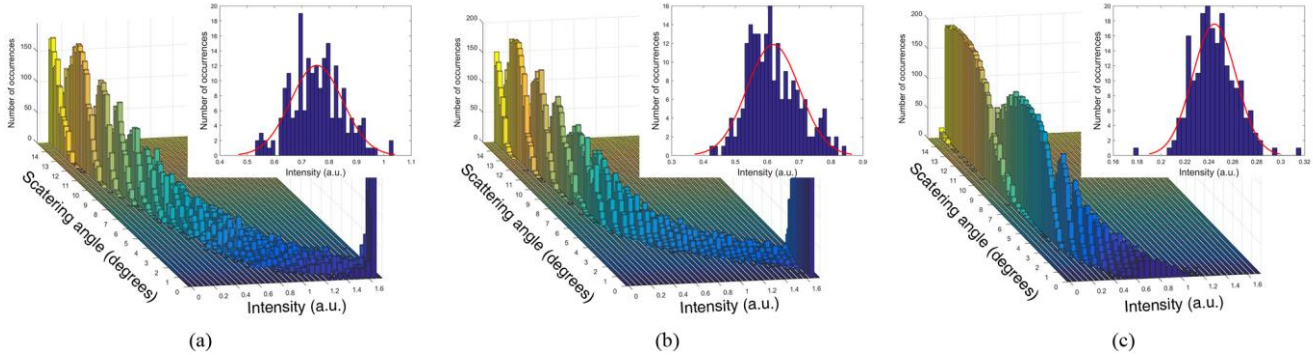

Fig. 12. 3D histogram plots showing the number of occurrences (z-axis) in 35 bin-grouped light intensity for each scattering angle measured. The insets show the distribution of bit-40 indicatively (a) 2 μm, (b) 4.8 μm and (c) 9.6 μm.

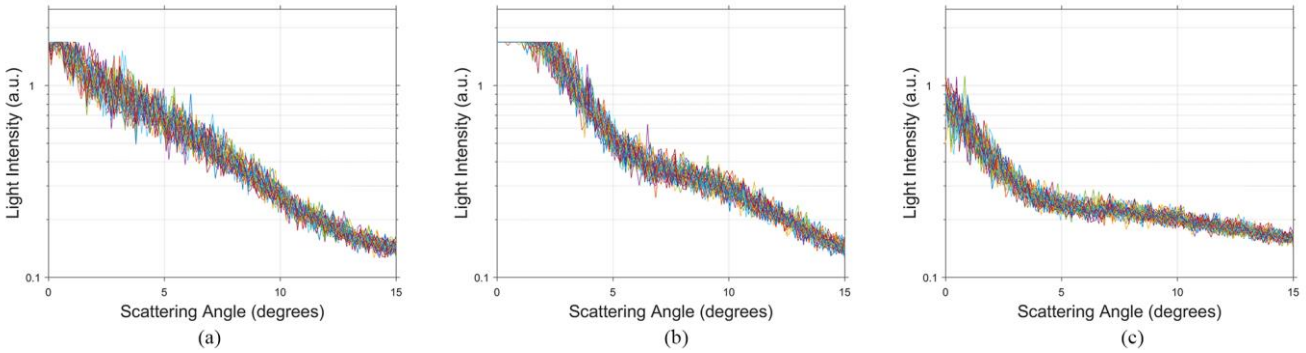

Fig. 13. Repeatability of the measurements for each particle size (a) 2 μm, (b) 4.8 μm and (c) 9.6 μm

in 35 bins and the number of occurrences respectively. The insets in each diagram show a histogram, using also 35 bins with a normal distribution fit (plotted as a red line), indicatively for bit No 40 (approximately 4° of scattering angle). The mean value and the variance of this bit for 2 μm, 4.8 μm and 9.6 μm particle diameters is $\bar{x}_2$=0.7545 and σ_2^2=0.0091, $\bar{x}_{4.8}$=0.6187 and $\sigma_{4.8}^2$=0.0067, $\bar{x}_{9.6}$=0.2446 and $\sigma_{9.6}^2$=0.0003 respectively. It is evident that the measured data follow significantly the normal distribution with a remarkably low deviation.

Fig. 13 demonstrates the 50 frames that were randomly chosen for each particle size, as mentioned in the previous section. Along with Fig. 12 it shows that the implemented system also presents significant repeatability, demonstrating a reliable distinguishing ability among these particle sizes.

4.4 Measurements over time

In in-vivo measurements, sampling over time is an important capability because it can allow the observation of dynamic events such as the changes of blood's volume inside the tissue's microvascular bed due to the blood flow. Such mechanism can be exploited for amplifying the scattering signal emerging from blood, similarly to pulse oximetry, as also explained in the introduction.

The performance of the system was tested for framerates up to 350 frames per second (clocking test results not shown

here). Higher rates are nominally possible and given the sub μs conversion time of the ADC, the framerate is only limited by the exposure time which was 38 μs in the presented scattering experiments. In order to evaluate the capability of the system for dynamic measurements under more light intensity - demanding conditions, scattering measurements were performed on the finger of an adult athlete at rest, for sampling periods of five seconds. After light intensity calibration runs, it was found that an integration time of 1 ms was suitable, in order to acquire a strong enough signal without leading the PDA sensor to saturation. Indicative results are presented in Fig. 14, using a framerate of 40 frames per second. The contraction of the finger's capillaries is clearly visible, corresponding to the athlete's heart pulse which was 60 bpm during measurements. In addition, in the marked circles the dicrotic notch is appearing clearly on each pulse. These results demonstrate the ability of the device to obtain measurements over time and detect pulse profiles.

Preliminary experimental results of scattering from two real blood samples, containing different blood cell concentrations, are indicatively shown in the inset of Fig. 14.

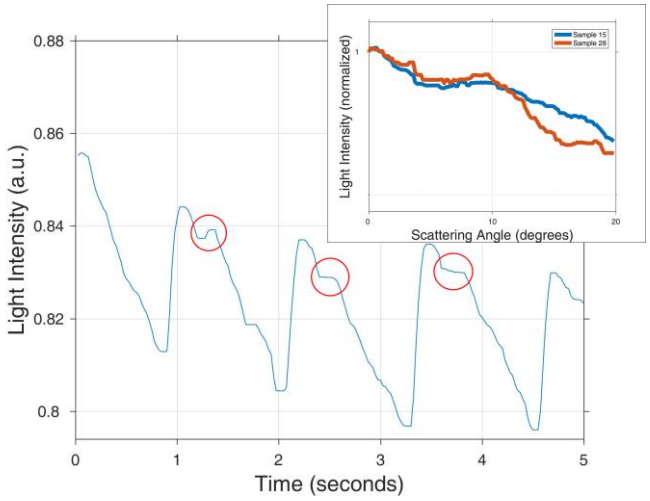

Fig. 14. Experimental measurements over time, showing the average intensity across the PDA sensor, through the finger of an adult athlete. A pulse rate of 50 bpm is clearly observed. The inset shows experimental data of Mie scattering from real blood samples.

5. Conclusion

In this paper, a portable system for studying light scattering on blood cells was presented. The system was tested by analysing calibration polystyrene microparticle solutions with sizes almost equivalent to those of blood cells. The capability of reliably distinguishing among solutions with different particle sizes from their scattering angle profile was demonstrated, without the use of optical processing. The weak Mie scattering profile is attributed to multiple scattering events. While the distinguishing capability focuses on blood cells, the detection of sizes in the 1 μm range and higher resolution (below 1 μm) is expected by extending the measured angle range and similar data analysis on other calibration particle sizes. The particle size detection ability is fundamentally limited to the light wavelength, while resolution is expected to be restricted by the Mie-scattering to diffusion signal ratio and data analysis capability. Using this sensor platform, optical filtering methods such as polarization gating, confocal microscopy and interferometry could be evaluated in order to enhance the Mie scattering signal. The sampling over time capability of the sensor is adequate for observing hemodynamic events, allowing the employment of differential pulse measurement and other dynamic measurements methods. The demonstrated features of the proposed device show promise for integrating state-of-the-art laboratory biomedical imaging techniques into portable non-invasive blood monitoring sensors.

While the proposed system demonstrates a size-distinguishing capability, differentiation among different-type, similar-size cells would expand the potential applicability of the system. Towards this direction, the consideration of the refractive index effect to Mie scattering in measured data analysis and the combination of the system with spectroscopic methods, for instance by using multiple wavelength sources or a prism-grating approach would be highly promising.

Declaration of Competing Interest

The authors declare that they have no known competing financial interests or personal relationships that could have appeared to influence the work reported in this paper.

Appendix A. Supplementary data

Supplementary data to this article can be found online at https://doi.org/10.1016/j.mee.2019.111129.

References

[1] R. Hovorka, Closed-loop insulin delivery: from bench to clinical practice, *Nature Reviews Endocrinology*, Review Article vol. 7, p. 385, 2011.

[2] J. Kim, A. S. Campbell, and J. Wang, Wearable non-invasive epidermal glucose sensors: A review, *Talanta*, vol. 177, no. Supplement C, pp. 163-170, 2018.

[3] A. Tura, A. Maran, and G. Pacini, "Non-invasive glucose monitoring: Assessment of technologies and devices according to quantitative criteria," *Diabetes Research and Clinical Practice*, vol. 77, no. 1, pp. 16-40, 2007.

[4] J. M. Goldman, M. T. Petterson, R. J. Kopotic, and S. J. Barker, "Masimo signal extraction pulse oximetry," (in eng), *J Clin Monit Comput*, vol. 16, no. 7, pp. 475-83, 2000.

[5] Z. Lu, X. Chen, Z. Dong, Z. Zhao, and X. Zhang, "A Prototype of Reflection Pulse Oximeter Designed for Mobile Healthcare," *IEEE Journal of Biomedical and Health Informatics*, vol. 20, no. 5, pp. 1309-1320, 2016.

[6] S. N. El-Beshbishi, K. E. Shattuck, A. A. Mohammad, and J. R. Petersen, "Hyperbilirubinemia and Transcutaneous

Bilirubinometry," *Cl. Chem.*, vol. 55, no. 7, pp. 1280-87, 2009.

[7] I. Fine and A. Finarov, "Probe for use in non-invasive measurements of blood related parameters," *ed: Google Patents*, 2006.

[8] M. Hammer, D. Schweitzer, B. Michel, E. Thamm, and A. Kolb, "Single scattering by red blood cells," (in eng), *Appl Opt*, vol. 37, no. 31, pp. 7410-8, 1998.

[9] C. F. Bohren, D. R. Huffman, "Absorption and Scattering by a Sphere" in *Absorption and Scattering of Light by Small Particles*, Weinheim DE, Wiley-VCH, 2007, ch.4, pp. 82–129.

[10] C. Iosifidis, K. Katsaliaki, P. Kollensperger, and M. E. Kiziroglou, "Design of an embedded sensor system for measuring laser scattering on blood cells," *in SPIE Microtechnologies*, 2017, vol. 10247, p. 7: SPIE.

[11] P. Laven, "MiePlot: a computer program for scattering of light from a sphere using Mie theory & the Debye series, http://www.philiplaven.com/mieplot.htm," ed.

[12] L. J. Steven, "Optical properties of biological tissues: a review," *Ph. in Med. and Biology*, vol. 58, no. 11, p. R37, 2013.

[13] T. J. Farrell, M. S. Patterson, and B. Wilson, "A diffusion theory model of spatially resolved, steady-state diffuse reflectance for the noninvasive determination of tissue optical properties in vivo," *Med. Ph.*, vol. 19, no. 4, pp. 879-888, 1992.

[14] A. Da Silva, C. Deumié, and I. Vanzetta, "Elliptically polarized light for depth resolved optical imaging," *Biomedical Optics Express*, vol. 3, no. 11, pp. 2907-2915, 2012.

[15] A. Wax, C. Yang, V. Backman, M. Kalashnikov, R. R. Dasari, and M. S. Feld, "Determination of particle size by using the angular distribution of backscattered light as measured with low-coherence interferometry," *Journal of the Optical Society of America A*, vol. 19, no. 4, pp. 737-744, 2002.

[16] H. Fang et al., "Confocal light absorption and scattering spectroscopic microscopy," *Applied Optics*, vol. 46, no. 10, pp. 1760-1769, 2007.

[17] S. V. Ravikant, "Determination of optical scattering properties of tissues using reflectance-mode confocal microscopy," *Scholar Archive*, vol. 861, 2012.

[18] V. Backman et al., "Measuring cellular structure at submicrometer scale with light scattering spectroscopy," *IEEE J. of Sel. T. in Quan. Elec.*, vol. 7, no. 6, pp. 887-893, 2001.

[19] J. W. Pyhtila et al., "In situ detection of nuclear atypia in Barrett's esophagus by using angle-resolved low-coherence interferometry," *Gastr. End.*, vol. 65, no. 3, pp. 487-91, 2007.

[20] P. Pagliaro, A. Belardinelli, V. Boko, P. Salamon, S. Manfroi, and P. L. Tazzari, "A non-invasive strategy for haemoglobin screening of blood donors," *Blood Transfusion*, vol. 12, no. 4, pp. 458-463, 2014.

[21] M. Pinto, M. L. Barjas-Castro, S. Nascimento, M. A. Falconi, R. Zulli, and V. Castro, "The new noninvasive occlusion spectroscopy hemoglobin measurement method: a reliable and easy anemia screening test for blood donors," (in eng), *Transfusion*, vol. 53, no. 4, pp. 766-9, 2013.

[22] "TSL1401CL 128 × 1 LINEAR SENSOR ARRAY WITH HOLD," 2011.

[23] T. Instruments, "AM335x ARM® Cortex™-A8 Microprocessors (MPUs)," 2011.

[24] Analog. (2018). LT1810 Dual 180MHz, 350V/µs Rail-to-Rail Input and Output Low Distortion Op Amps *http://www.analog.com/en/products/lt1810.html*

[25] D.-G. f. R. a. Innovation, The certification of monodisperse latex spheres in aqueous suspensions with nominal diameters of 2,0 mm, 4,8 mm and 9,6 mm (Reference materials No 165, 166 and 167). *EU Publications*, 1996.

[26] S. H. Jones, M. D. King, and A. D. Ward, "Determining the unique refractive index properties of solid polystyrene aerosol using broadband Mie scattering from optically trapped beads," , *Phys Chem Chem Phys*, vol. 15, no. 47, pp. 20735-41, 2013.

[27] M. Daimon and A. Masumura, "Measurement of the refractive index of distilled water from the near-infrared region to the ultraviolet region," (in eng), *Appl Opt*, vol. 46, no. 18, pp. 3811-20, 2007.